Science

AAAS

Eddy-Driven Stratification Initiates North Atlantic Spring Phytoplankton Blooms
Amala Mahadevan *et al.*
Science **337**, 54 (2012);
DOI: 10.1126/science.1218740

This copy is for your personal, non-commercial use only.

Eddy-Driven Stratification Initiates North Atlantic Spring Phytoplankton Blooms

Amala Mahadevan,[1] Eric D'Asaro,[2]* Craig Lee,[2] Mary Jane Perry[3]

Springtime phytoplankton blooms photosynthetically fix carbon and export it from the surface ocean at globally important rates. These blooms are triggered by increased light exposure of the phytoplankton due to both seasonal light increase and the development of a near-surface vertical density gradient (stratification) that inhibits vertical mixing of the phytoplankton. Classically and in current climate models, that stratification is ascribed to a springtime warming of the sea surface. Here, using observations from the subpolar North Atlantic and a three-dimensional biophysical model, we show that the initial stratification and resulting bloom are instead caused by eddy-driven slumping of the basin-scale north-south density gradient, resulting in a patchy bloom beginning 20 to 30 days earlier than would occur by warming.

Springtime phytoplankton blooms in high- and mid-latitude oceans contribute substantially to global photosynthetic fixation and export of carbon from the surface ocean, with the North Atlantic alone accounting for 20% of net global CO_2 uptake (1). During winter, strong surface cooling and winds drive turbulent mixing that repeatedly carries phytoplankton to depths of several hundred meters, well below the lighted surface layer. Combined with low solar radiation, these factors limit winter phytoplankton growth. Springtime increases in solar radiation, coupled with weakening surface forcing and shallowing mixing depths (2, 3), cause the surface sunlit layer to retain phytoplankton for longer periods, promoting rapid growth that outcompetes grazing and leads to a phytoplankton bloom.

Vertical density stratification exerts a fundamental control on mixing depth, with strong stratification suppressing turbulence and reducing the depth of mixing. Previous studies, employing one-dimensional (1D) (vertical) models, attribute springtime increases in stratification to surface warming by solar radiation and air-sea heat exchange (4, 5). This study demonstrates a 3D process in which 1- to 10-km scale instabilities growing from horizontal density gradients give rise to eddies that generate vertical stratification, thus initiating a spring bloom earlier than expected from solar heating.

Deep wintertime mixed layers (MLs), though homogenized vertically, have a horizontal density gradient with heavier (colder) water toward the north and lighter (warmer) water southward (Fig. 1 and Fig. 2, B and D). In a nonrotating

system, the heavy northern waters would slide laterally under lighter southern waters, creating vertical stratification and releasing potential energy stored in the horizontal density gradient. However, Earth's rotation inhibits such movement (6), instead inducing flow normal to the horizontal density gradient that preserves both stored potential energy and deep MLs. Recent work has shown that the growth of instabilities (7) within the ML can tap this potential energy to develop energetic eddies, initially 1 to 10 km in horizontal extent and as deep as the ML. These eddies drive net horizontal transfer of lighter water above heavier water that can stratify the ML (8) on a time scale of weeks (Fig. 1 and movie S1). This process of ML eddy restratification competes with vertical mixing due to surface wind and cooling to set the density structure of the ML. High-resolution process-study models that resolve small ML eddies suggest that eddy-driven restratification is important for light-limited phytoplankton blooms in the Mediterranean (9, 10) and at high-latitude ocean fronts (11). Although parameterizations of ML eddy restratification developed from such studies (8) greatly improve the predictions of ML depth in climate models (12), direct observations of ML eddy restratifi-

cation (13) have been limited. This study provides observational evidence for springtime stratification by ML eddies and, with the use of a numerical model in the observational setting, shows that the process affects the timing and structure of the North Atlantic spring phytoplankton bloom.

Observations. In the spring of 2008, an intensive observational program (14) characterized the initiation and development of the spring phytoplankton bloom south of Iceland (Fig. 2A). North Atlantic Bloom 2008 (NAB08) measurements were collected in a patch-following reference frame defined by an autonomous, subsurface Lagrangian float (15). Four Seaglider robots—self-propelled, buoyancy-driven autonomous underwater vehicles—surveyed around the float. The array of autonomous instruments was deployed from R/V *Bjarni Saemundsson* on 4 April 2008 (yearday 95; yearday 1 = 1 January 2008), augmented by detailed measurements of physics, biology, and chemistry from R/V *Knorr* in May. Our analysis uses measurements of potential density from all seven platforms; chlorophyll concentration additionally includes Moderate Resolution Imaging Spectroradiometer (MODIS) satellite data (see supplementary materials and methods). Potential density profiles obtained from Argo floats that sampled this region between 2000 and 2009 provide a climatological picture.

In early April 2008, potential density ρ profiles (Fig. 3A) showed well-mixed layers 200 to 300 m deep, with ρ increasing toward the north (y direction) in both NAB08 measurements (Fig. 2B) and climatology (Fig. 2D). The lateral density gradient ρ_y was composed of a series of fronts with large ρ_y, interspersed with regions of more laterally uniform density (Fig. 2B). Vertical stratification increased dramatically during the measurement period, so that by late May the mixed layer was often only 10 m thick (Fig. 3B). Buoyancy frequency $N^2 \equiv -(g/\rho_0)\partial\rho/\partial z$ (where g is the acceleration due to gravity and ρ_0 is a reference density), a function of the vertical density gradient, provides a quantitative measure of stratification, which we averaged over shallow (0 to 100 m) and deep (100 to 300 m) ranges.

Springtime stratification develops in two distinct phases. Deep wintertime MLs initially
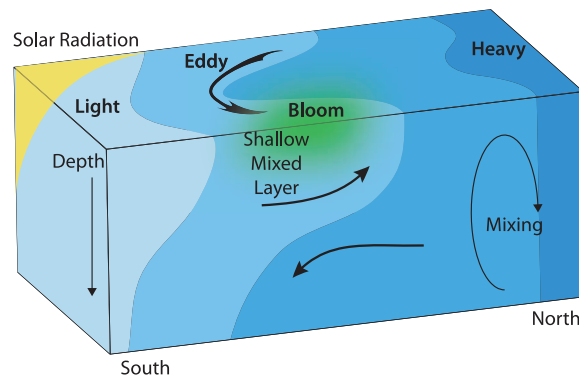
Fig. 1. In early spring, the deep, well-mixed layers created during the winter are denser to the north. Eddies move heavier water south and downward and lighter water north and upward, creating patches of shallow MLs that retain phytoplankton within the upper sunlit region and initiate the spring bloom. [Graphic by K. Mahadevan]

progress from well mixed to linearly stratified across the upper 200 to 300 m (Fig. 3A, blue to orange profiles). Average N^2 in both the shallow (Fig. 3B, solid lines) and deep (dashed) layers is small in midwinter and increases concurrently to about 3×10^{-6} s^{-2} between yeardays 100 and 125. A strong storm produced the short-lived decrease in NAB08 stratification near yearday 120. In the second phase, stratification in the shallow layer increases sharply, diverging from the deep layer. Both the NAB08 data (Fig. 3B, red) and the climatological Argo data (Fig. 3B, green) show this pattern, albeit with somewhat different timings.

The observations suggest that ML eddies introduce the initial stratification across the entire depth of the wintertime mixed layer, whereas surface warming acts later and increases only shallow stratification. Estimates of air-sea heat flux Q [National Oceanography Centre (NOC) 1.1a climatology (16) (supplementary materials, section 1.8)] indicate that the atmosphere cooled the ocean until roughly yearday 120 (Fig. 3D). During this period, the temperature measured by the

float decreased by 0.4°C, a rate roughly consistent with the heat fluxes in Fig. 3D and measured ML depths (fig. S10). Thus, the first phase of stratification occurs during a period of surface cooling and entails a vertical density difference of 0.12 kg m^{-3} (Fig. 3A), which is the same as the lateral density change over ~250 km (Fig. 2B). The initial increase in stratification spans the upper 200 to 300 m and is produced by a layering of warm, salty water of southern origin atop colder, fresher waters originating from the north. These features are consistent with the formation of vertical stratification by eddy-driven slumping of the lateral gradient. Net surface heating starts on yearday ~120, which is approximately when the second, surface-intensified phase of stratification begins. Thus, both the magnitude and timing of the heat flux and the horizontal and vertical structure of the upper ocean support the hypothesis that ML eddies drive the initial restratification.

As postulated by Sverdrup (17), initiation of the spring phytoplankton bloom occurs concurrently with the observed onset of stratifica-

tion. Chlorophyll concentration (a surrogate for phytoplankton biomass), which is measured by autonomous, ship-based, and MODIS satellite sensors, remained at low levels in midwinter, then increased rapidly between yeardays 110 and 130, marking the onset of the spring bloom (Fig. 3C). Diatoms dominated the bloom, which terminated (18, 19) due to exhaustion of silicate, an essential nutrient for diatoms. This study focuses on the initiation and evolution of this diatom bloom, up to the time of silicate limitation.

Theory. Competition between the stratifying effects of ML eddies and the destratifying effects of surface cooling modulated by wind forcing governs the development of stratification within the ML in winter. Lateral density gradients within the surface ML are unstable (7, 20) and generate ML eddies, which move parcels of heavy water southward and downward and parcels of light water north and up (Fig. 1). The overall effect of the eddies is to convert the horizontal density gradient into vertical stratification. Convective mixing, driven by surface
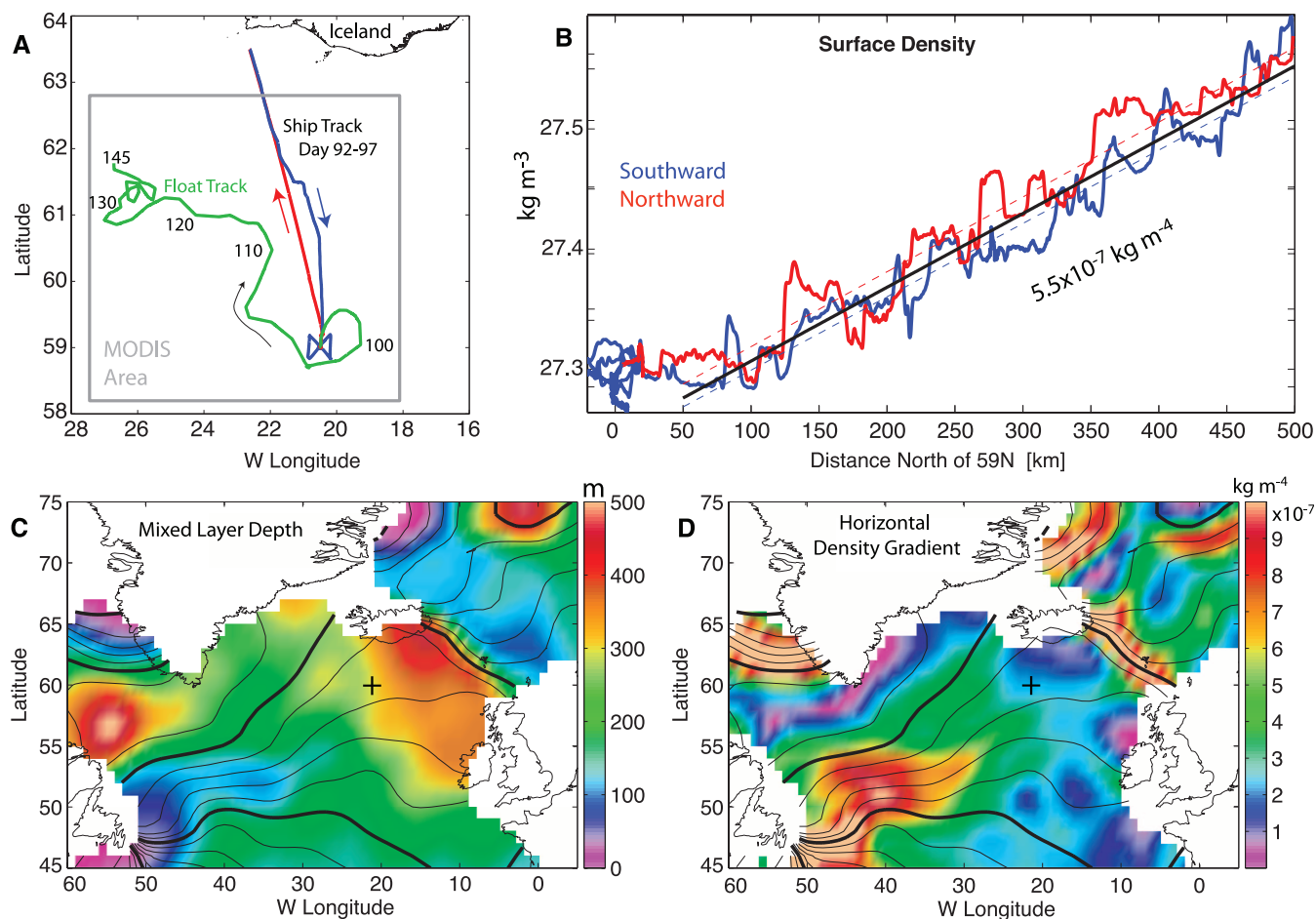

Fig. 2. (A) Experimental region showing the Lagrangian float track (green) labeled by yearday and the deployment cruise track (blue, southward; red, northward). The gray box demarcates the region of averaged MODIS satellite chlorophyll in Fig. 3C. **(B)** Surface density along the ship track, colored as in (A). Dashed lines give fits for inbound and outbound tracks; the solid black line fits both. Slope differences are less than 2%. Maps of **(C)** ML depth and **(D)** magnitude of horizontal density gradient from 1997-to-2009 Argo data (35), smoothed with Gaussian scales of 2° latitude and 3° longitude, both with contours of density (contour interval of 0.1 kg m^{-3}). Black crosses denote the approximate experimental location.

cooling, counters the effects of ML eddies by homogenizing the water column and destroying vertical gradients. In the presence of Earth's rotation, winds induce a surface Ekman transport normal and to the right of the wind in the Northern Hemisphere. Thus, a wind along the density front in the direction of the frontal current ("downfront") drives heavy water over light, producing convective mixing similar to that driven by surface cooling (*21*). The balance between restrati-

fying mechanisms (for instance, ML eddies, solar heating, and up-front winds) and mixing (due to, for example, surface cooling and down-front winds) controls ML depth.

The stratifying buoyancy flux due to ML eddies (*8*) for a single front is proportional to $(b_y H)^2/f$, where H is the ML depth, b_y is the initial meridional gradient of the buoyancy $b = -g (\rho - \rho_0)/\rho_0$ at a front, and f is the Coriolis frequency. The ratio of the buoyancy fluxes due to cooling (de-

stratifying) and ML eddies (stratifying) is estimated as $S = \frac{-g\alpha}{0.06\rho_0 C_p} \frac{fQ}{b_y^2 H^2}$, where Q, α, and C_p are the air-sea heat flux, thermal expansion coefficient, and specific heat capacity of seawater, respectively. We choose $b_y \sim -0.3 \times 10^{-7} \text{s}^{-2}$, a value close to the density gradient along the tracks in Fig. 2B. With $H \sim 300$ m, $C_p = 3988$ J/kg/°K, $f = 1.28 \times 10^{-4}$ s^{-1}, $\rho_0 = 1025$ kg/m^3, and $\alpha = 1.6 \times 10^{-4}$ °K^{-1}, we estimate that $S = 1$ would be achieved at $Q \sim -100$ W/m^2. This implies that, in
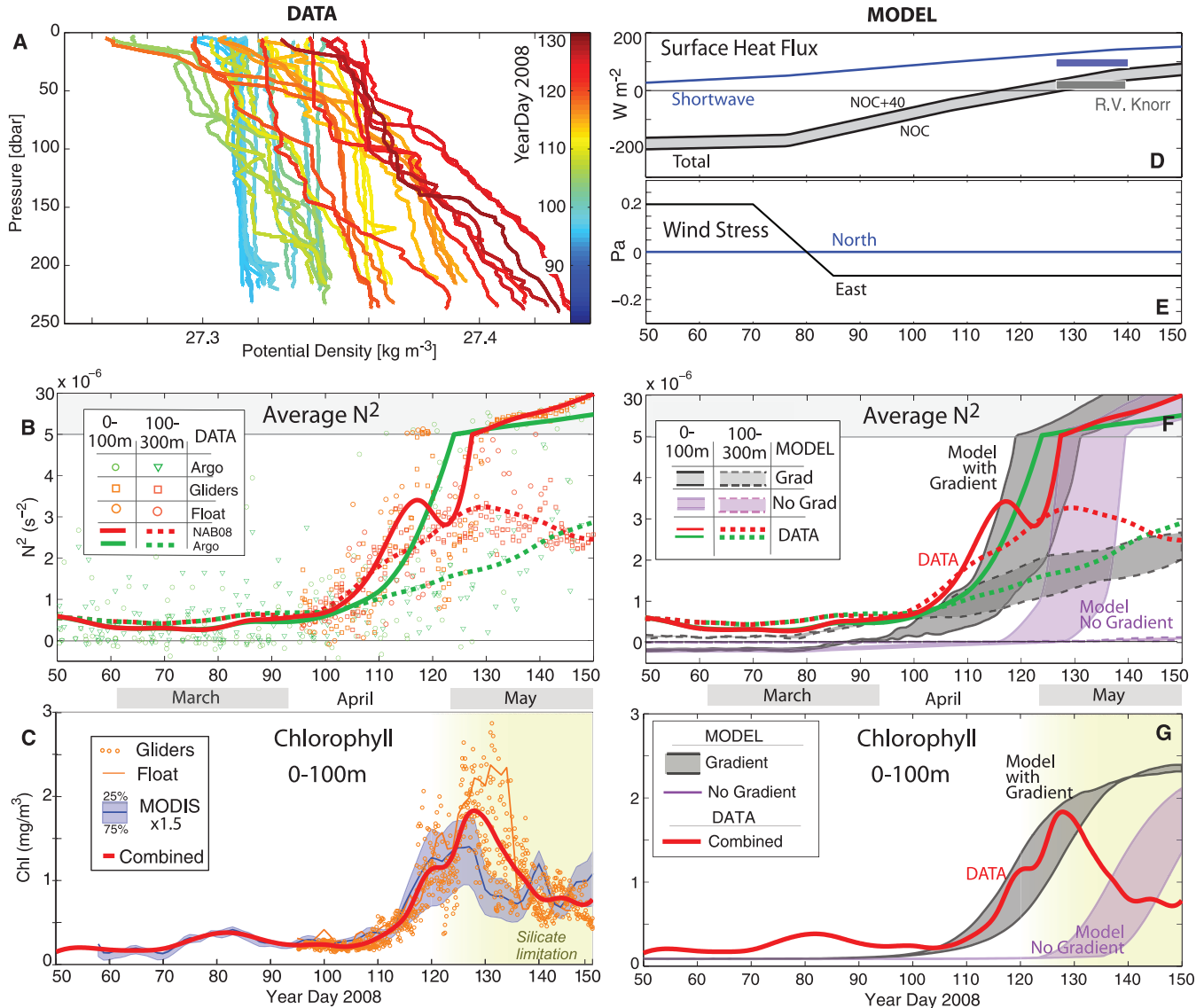

Fig. 3. Comparison of data (left column) and model (right column). (**A**) Evolution of vertical profiles of potential density at the float. Line color denotes time (yearday 2008). (**B**) Stratification, average value of N^2, as measured by Argo floats (green), gliders (NAB08; red), and Lagrangian float (NAB08; orange) between 0 and 100 m and 100 and 300 m. Lines (solid, 0 to 100 m; dashed, 100 to 300 m) are smoothing spline fits to the Argo (green) and NAB08 (red) data. (**C**) Chlorophyll (Chl) 0 to 100 m from float (orange line), Seagliders (dots), and MODIS satellite (blue with 25 and 75 percentiles) from within the gray box of Fig. 2A, multiplied by 1.5 to calibrate to observations. Smoothing spline (heavy red line) is fit to all data. Yellow shading indicates the onset of silicate limitation in the data. (**D**) Air-sea heat flux; total (black) and shortwave (blue) components from NOC climatology (see supple-

mentary materials). NOC plus 40 W m^{-2} (NOC + 40) shows the range of uncertainty. Short, thick lines indicate average values from the R/V *Knorr* cruise. (**E**) Wind stress used to drive the model derived from WaveWatch III (see supplementary materials), eastward (black) and northward (blue) components. (**F**) Model stratification (average N^2 over layer) from runs with lateral density gradient (shaded gray) and without (purple) for 0- to 100-m (solid) and 100- to 300-m (dashed) layers. The shaded regions indicate a range of model solutions obtained by increasing the NOC heat flux by 40 W m^{-2} to account for uncertainty in the heat flux estimate. Red and green curves from observations in (B) are overlaid. (**G**) Model chlorophyll concentration in the upper 100 m (average), colored as in (F). Chlorophyll from the combination of observations in (C) is overlaid.

the absence of winds, ML eddies would overcome cooling-induced mixing and restratify the ML (that is, $S < 1$) when the cooling weakens beyond the -100 W/m^2 threshold. Down-front winds also counter restratification by ML eddies, and a similar scaling estimate (*22*) for the ratio of buoyancy fluxes due to down-front winds and ML eddies is given by $S_w = \frac{\tau}{0.06\rho_0 b_y H^2}$, where τ is the down-front surface wind stress. $S_w = 1$ corresponds to $\tau = 0.17$ Pa.

Variations of parameters S and S_w can qualitatively explain the timing of the observed stratification during NAB08. Before yearday 70, strong surface cooling ($Q \sim -200$ W/m^2) and down-front winds ($\tau = 0.2$ Pa) easily overcame ($S > 1$, $S_w > 1$) restratification by ML eddies. Consequently, the ML remained well mixed. Near yearday 80, persistent eastward (down-front, $S_w > 1$) winds shifted westward (up-front, $S_w \sim 1$). Near yearday 100, surface cooling declined to below -100 W/m^2 ($S \leq 1$), which is roughly when ML stratification started to increase. Thus, theory suggests that the mixed layer restratified because of the decrease in surface cooling, aided by the switch in wind direction from eastward to westward. However, uncertainties in the scaling parameters in these simple formulas, as well as the complexities of their combined effects, require a more detailed evaluation of this hypothesis through modeling.

Modeling. We conducted a more quantitative analysis of this mechanism with the use of a 3D process-study ocean model (*23*) coupled to a single-species, light-limited phytoplankton model (supplementary materials sections 1.4 to 1.9). The domain, encompassing several of the many small fronts seen in Fig. 2B, is 480 km (north-south) by 96 km (east-west, periodic). The model is initialized in midwinter (yearday 30), with three fronts spanning the domain, and evolves for 120 days. By yearday 95, the start of our observations, the model has evolved to an equilibrium condition with little resemblance to the initial conditions (supplementary materials section 1.7 and fig. S6). The north-south average gradient b_y, wave number spectrum of b_y, and probability density function of b_y are close to those found along the observed transect in Fig. 2B (figs. S7 and S8). The model is slightly smoother than the observations, underestimating the mean square b_y by ~50%, which would slow the model's restratification rate by ~20% (supplementary materials section 1.7), but this error is less than other uncertainties in the model.

The model is forced (Fig. 3, D and E, details in the supplementary materials) by a uniform surface wind stress and a surface heat flux from the NOC 1.1a climatology (*16*), which cools slightly more strongly toward the north. Bagniewski *et al.* (*24*) optimized an ecosystem model to fit observations of light, chlorophyll, particulate carbon, nitrate, and silicate made by (or near) the NAB08 Lagrangian float. These data were sufficient to strongly constrain the phytoplankton model parameters. Model components related to nutrient limitation and grazing were removed, leaving a single group of modeled phytoplankton limited only by light. This is appropriate for the early part of the bloom where nutrient limitation and grazing play a minor role in the full model. Before the onset of the bloom, the average phytoplankton in the ML is restored toward a seed population with 0.08 mg m^{-3} of chlorophyll, based on observations at the start of NAB08. Details of the model and comparisons with data can be found in the supplementary materials and also in (*24*).

Results from four model simulations, two of which generate ML eddies due to the presence of a horizontal density gradient ("Gradient" cases in Fig. 3), and two control runs, which do not ("No Gradient" cases in Fig. 3), characterize the impact of ML eddies. Two ML eddy simulations using the NOC heat flux (supplementary materials and methods and figs. S5 and S6) and NOC plus 40 W/m^2 (Fig. 3D) span the uncertainty in heat flux. The controls are identical to these, but initialized with no lateral density gradients and thus have no ML eddies. Additional simulations vary wind and heat flux (supplementary materials section 2, fig. S9, and table S1).

The two ML eddy simulations (Fig. 3F, shaded) reproduce the two phases of stratification seen in the data. The first phase stratifies both the shallow and deep layers starting near yearday 90; the second phase strongly stratifies the shallow layer starting at yearday 110 to 120. These results agree with the observations to within the uncertainties due to heat flux (shading) and interannual variability [differences between NAB08 (red) and climatology (green)]. The slight divergence between the rate of increase of stratification in the upper and lower layers before day 120 is also reproduced in the model. They also reproduce the concurrent increase in chlorophyll (Fig. 3G, shaded) around yearday 110. After roughly yearday 130, the modeled and observed chlorophyll diverge due to the onset of silicate limitation, which is not included in the model. The "No Gradient" control cases, (Fig. 3F, purple) predict no increase in stratification until the heat flux turns positive near yearday 120 and no increase in chlorophyll (Fig. 3G, purple) until about yearday 130. These model simulations indicate that the initial stratification of the wintertime ML and the onset of the bloom before atmospheric warming are due to ML eddies arising from horizontal ML density gradients. In their absence, the stratification and bloom would be delayed by 20 to 30 days.

The North Atlantic spring bloom is patchy (*25*), as seen in a satellite chlorophyll image (Fig. 4B) and in the spread of the float and Seaglider chlorophyll data (Fig. 3C, compare orange dots
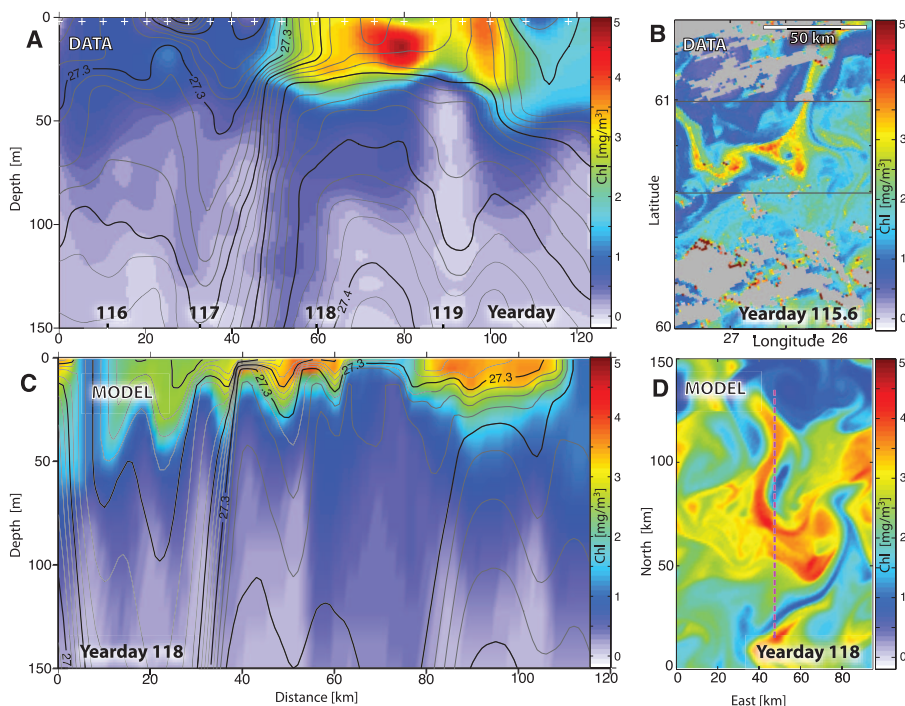

Fig. 4. Spatial structure of bloom in data (top row) and from model (bottom row). (**A**) Seaglider section, with chlorophyll (color) and potential density (contours). The finest contour interval is 0.00625 kg m^{-3}. Small white crosses mark profile locations. Data are smoothed over ~7 km horizontally. The horizontal axis is either distance along track (x axis) or time (black numbers). (**B**) MODIS satellite chlorophyll (yearday 115.6) multiplied by 1.92, the product of 1.5 (as in Fig. 3C) and 1.28, to account for the average chlorophyll increase between yeardays 115.6 and 118. Gray denotes clouds. (**C**) Model section across chlorophyll patches on yearday 118 plotted as in (A). (**D**) Model surface chlorophyll on yearday 118 plotted as in (B). The dashed vertical line shows the location of the section in (C).

and line). A measured vertical-horizontal section during bloom growth (Fig. 4A) shows steeply sloping density surfaces with regions of high and low stratification. Near-surface chlorophyll is greatest above the strong stratification (26), where the reduced depth of mixing leads to greater light exposure and more phytoplankton growth. A significant correlation exists between the spatial variations in chlorophyll and stratification in the upper 100 m (fig. S16) during the period of rapid growth (yeardays 110 to 116). A model section (Fig. 4C) shows similar vertical and horizontal structures. Plots of surface chlorophyll from data (Fig. 4B) and the model (Fig. 4D) show kilometer-scale filaments of high and low chlorophyll. Wave number spectra of chlorophyll (fig. S15) from the model and from the image in Fig. 4 have similar shapes: white at 100-km wavelength steepening to a –2 slope at the 10-km wavelength. Observations and simulations exhibit similar patchiness, with variations in stratification and phytoplankton biomass occurring on similar scales.

Discussion. Several recent studies have proposed alternate hypotheses for the initiation of spring blooms, but these theories do not explain our observations. Taylor and Ferrari (11) suggest that the bloom occurs when the ML turbulence decreases, allowing phytoplankton to grow within a deep, but weakly mixed layer. The vertical motion of the Lagrangian float directly measures the vertical velocity (27) and, thus, the intensity of the turbulence. The root mean square vertical velocity is strongly correlated with wind stress, neither of which decreased very much at the time of the bloom (fig. S17A). Furthermore, this mechanism acts by creating strong vertical gradients of plankton within the ML, which are not observed (supplementary materials section 5 and fig. S17B). Taylor and Ferrari (3) also suggest that symmetric instability (SI) could produce vertical stratification from horizontal gradients. However, the amount of stratification that SI could produce is very small compared with ML eddies (supplementary materials section 5.2). Furthermore, it is not dominant during the stratification phase, because the direction of the wind relative to front (28), surface cooling, and density-velocity structure are not favorable. Alternatively, Behrenfeld (29) suggests that a deepening ML dilutes plankton, decreasing the interaction rate between phytoplankton and zooplankton, reducing grazing, and thus allowing phytoplankton to grow. The NAB08 bloom occurs during a period of shallowing ML depth, so this mechanism does not apply.

Blooms driven by ML eddy restratification evolve differently from those driven by surface heating. The timing of a bloom caused by eddy restratification depends on the lateral density gradient, ML depth, the decrease in surface cooling below a threshold value, and wind speed and direction. In contrast, the timing of a bloom caused by surface heating depends on the onset of heating and on wind strength (mixing rate), but not on wind direction. Differences in forcing functions between these two mechanisms suggest that the response of bloom onset to interannual and climatic changes could depend strongly on which mechanism prevails.

Blooms initiated by ML eddies can be expected to have patchier growth (fig. S12) and greater spatial heterogeneity at the 1- to 10-km scale than those initiated by surface heating, as the former introduces more horizontal gradients. This heterogeneity may allow a more diverse planktonic community with different species dominating in different patches (30). Even in midwinter, the ML eddies could generate intermittent patches of shallow stratification, as seen in the Argo float data (Fig. 3B), leading to enhanced winter productivity (29) and the maintenance of seed populations for the spring bloom (31).

The ML eddies that initiate the bloom also transport water vertically along the sloping isopycnals, bringing nutrient-rich water from across the entire wintertime ML intermittently into the euphotic zone (Fig. 4A). In contrast, blooms caused by surface heating alone will be confined to the shallow surface layer, limiting access to and shading the nutrient-rich waters below. Thus although our simulations do not include nutrient effects, we anticipate that enhanced nutrient fluxes into surface waters due to ML eddies will lead to an overall increase in carbon fixation.

Eddy restratification is effective in this area of the Icelandic basin due to the existence of deep (200 to 400 m) MLs and substantial (1 to 5 × 10^{-7} kg·m^{-4}) average lateral density gradients (Fig. 2, C and D). Analysis of Argo float data for the January-to-April period (Fig. 2, C and D) shows similar conditions across most of the subpolar North Atlantic, with the westward shallowing of MLs compensated by increasing lateral gradients. These conditions are widespread in the subpolar oceans, suggesting that the ML eddy processes described here play a major role in controlling bloom timing in the subpolar North Atlantic (2) and in similar blooms globally.

Roughly half (32) of global net photosynthesis occurs in the ocean, with upper-ocean stratification playing a key role in regulating productivity. The current generation of climate models control springtime ML stratification exclusively by vertical processes. These results suggest that lateral processes driven by horizontal density gradients also play an important role, as the results affirm the need for parameterizing these processes (33) and their importance in controlling ocean productivity and the timing of phytoplankton blooms (3, 9, 11, 34).

References and Notes

1. C. L. Sabine et al., Science 305, 367 (2004).
2. D. A. Siegel, S. C. Doney, J. A. Yoder, Science 296, 730 (2002).
3. J. Taylor, R. Ferrari, Limnol. Oceanogr. 56, 2293 (2011).
4. J. J. Waniek, J. Mar. Syst. 39, 57 (2003).
5. S. A. Henson, I. Robinson, J. Allen, J. Waniek, Deep-Sea Res. Part I Oceanogr. Res. Pap. 53, 1601 (2006).
6. A. Tandon, C. Garrett, J. Phys. Oceanogr. 24, 1419 (1994).
7. G. Boccaletti, R. Ferrari, B. Fox-Kemper, J. Phys. Oceanogr. 37, 2228 (2007).
8. B. Fox-Kemper, R. Ferrari, R. Hallberg, J. Phys. Oceanogr. 38, 1145 (2008).
9. M. Lévy, L. Mémery, G. Madec, J. Mar. Syst. 16, 7 (1998).
10. M. Lévy, L. Mémery, G. Madec, Deep-Sea Res. Part I Oceanogr. Res. Pap. 46, 1137 (1999).
11. J. Taylor, R. Ferrari, Geophys. Res. Lett. 38, L23601 (2011).
12. B. Fox-Kemper et al., Ocean Model. 39, 61 (2011).
13. D. L. Rudnick, R. Ferrari, Science 283, 526 (1999).
14. K. Fennel, I. Cetinić, E. D'Asaro, C. Lee, M. J. Perry, Eos 92, 465 (2011).
15. E. A. D'Asaro, J. Atmos. Ocean. Technol. 20, 896 (2003).
16. J. P. Grist, S. A. Josey, J. Clim. 16, 3274 (2003).
17. H. Sverdrup, J. Cons. Cons. Int. Explor. Mer 18, 287 (1953).
18. P. Martin et al., Deep-Sea Res. Part I Oceanogr. Res. Pap. 58, 338 (2011).
19. M. B. Alkire et al., Deep-Sea Res. 64, 157 (2012).
20. P. H. Stone, J. Atmos. Sci. 27, 721 (1970).
21. L. Thomas, C. M. Lee, J. Phys. Oceanogr. 35, 1086 (2005).
22. A. Mahadevan, A. Tandon, R. Ferrari, J. Geophys. Res. 115, C03017 (2010).
23. A. Mahadevan, J. Oliger, R. Street, J. Phys. Oceanogr. 26, 1881 (1996).
24. W. Bagniewski, K. Fennel, M. J. Perry, E. A. D'Asaro, Biogeosciences 7, 1 (2010).
25. A. J. Watson, C. Robinson, J. E. Robinson, P. J. L. B. Williams, M. J. R. Fasham, Nature 350, 50 (1991).
26. E. Frajka-Williams, P. B. Rhines, C. C. Eriksen, Deep-Sea Res. Part I Oceanogr. Res. Pap. 56, 2144 (2009).
27. R. Harcourt, E. A. D'Asaro, J. Atmos. Ocean. Technol. 27, 1918 (2010).
28. E. D'Asaro et al., Science 332, 213 (2011).
29. M. J. Behrenfeld, Ecology 91, 977 (2010).
30. A. Bracco, A. Provenzale, I. Scheuring, Proc. Biol. Sci. 267, 1795 (2000).
31. J. Backhaus et al., Mar. Ecol. Prog. Ser. 251, 1 (2003).
32. P. Falkowski, Photosynth. Res. 39, 235 (1994).
33. B. Fox-Kemper, R. Ferrari, J. Phys. Oceanogr. 38, 1166 (2008).
34. S. Okamoto, T. Hirawake, S.-I. Saitoh, Deep-Sea Res. Part II Top. Stud. Oceanogr. 57, 1608 (2010).
35. J. Holte, L. Talley, J. Atmos. Ocean. Technol. 26, 1920 (2009).

Supplementary Materials